Analytical Methods

Accepted Manuscript

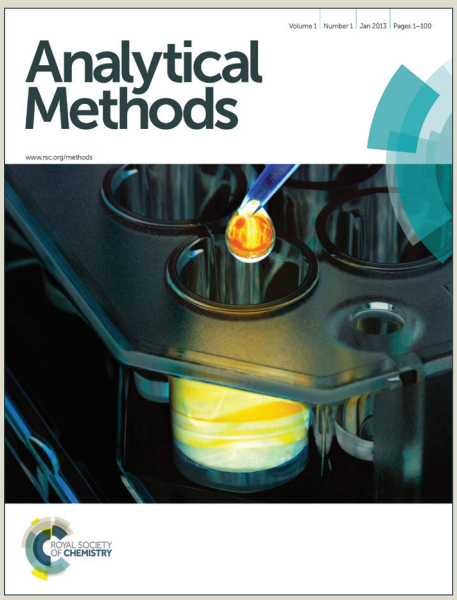

ROYAL SOCIETY OF CHEMISTRY

www.rsc.org/methods

Electrophysiological Analysis of Biopsy Samples using Elasticity as an Inherent Cell Marker for Cancer Detection

Azhar Ilyas,[abc] Waseem Asghar,[abc] Shahina Ahmed,[d]

Yair Lotan,[e] Jer-Tsong Hsieh,[e] Young-tae Kim [cd]

and Samir M. Iqbal,[*abcdf]

[a]Nano-Bio Lab, University of Texas at Arlington, Arlington, Texas 76019, USA

[b]Department of Electrical Engineering, University of Texas at Arlington, Arlington, Texas 76011, USA

[c]Nanotechnology Research Center, University of Texas at Arlington, Arlington, Texas 76019, USA

[d]Department of Bioengineering, University of Texas at Arlington, Arlington, Texas 76010, USA

[e]Department of Urology, University of Texas Southwestern Medical Center at Dallas, Dallas, Texas, 75390, USA

[f]Joint Graduate Committee of Biomedical Engineering Program, University of Texas at Arlington and University of Texas Southwestern Medical Center at Dallas, University of Texas at Arlington, Arlington, Texas 76010, USA

[*] To whom correspondence should be addressed:

Samir M. Iqbal, Ph.D.

500 S. Cooper Street, Room #217, University of Texas at Arlington, Arlington, TX 76019, USA

Phone: +1-817-272-0228

Fax: +1-817-272-7458

E-mail: smiqbal@uta.edu

Abstract

Biopsy samples from patients are valuable for diagnosis. A label-free approach for early diagnosis of cancer from biopsied sample is reported. The scheme relies on single solid-state micropore as the transducer component and the cell elasticity as the indicator of cell health. Biomechanical discrimination of cancerous cells depends on purely intrinsic properties and is not limited by the availability of biomarkers. As a model, bladder cancer cells showed specific electrical signatures, very different from healthy cells. The correlated detection of tumor cells was done with an efficiency of 75%. The difference in cellular elasticity gave one order of magnitude lower translocation time for tumor cells. The capability to recognize very few tumor cells solves the prime challenge in biopsy exams. A comparison of the motility and stiffness of cancer and normal urothelial cells showed distinctive quantifiable viscoelastic behavior.

Keywords: Elasticity; Translocation time; Focused ion beam; Biopsy sample; Cell mechanics; Cancer Diagnosis

Introduction

Over the last many decades, mortality rate from some cancers has been the highest. Within contemporary clinical settings, many of the cancers are usually diagnosed at advanced and incurable stages. Common diagnostic approaches vary between cancers. For example, for bladder cancer most common methods include biopsy, cytology, cytoscopy, and detection of immunological markers. These approaches have inadequacies such as flawed judgment (biopsy examination and cytology), high cost (cytoscopy), low sensitivity (cytology and immunological markers) and low specificity (cytoscopy).[1-3] Moreover, incapability of being used at point-of-care and lack of statistical comparison at single cell level limit the deployment of these methods in clinics. Therefore, a more reliable, rapid, and inexpensive detection scheme is critical to diagnose clinically significant but asymptomatic cancers.

Tissue or cell samples taken directly from the locale where tumor is suspected can be the best source to diagnose almost all types of cancer. The procedure used to obtain such sample is called *biopsy*. Open surgical biopsy or image-guided interventions obtain cancer cells of primary tumors from a precise region but entail risk of procedural complications.[4] Percutaneous biopsy is a typically used clinical procedure that includes fine needle aspiration (FNA) and core biopsy. FNA employs a very fine needle of 22-gauge (22G) to collect the sample for cytopathology whereas core biopsy uses a slightly larger needle of 16G or 19G to obtain a small tissue section for histology and immunohistochemical analysis.[5] The percutaneous biopsy has many benefits over open surgical procedures including patient compliance, fewer chances of serious complications, low cost and easy processing but it involves the risk of missing the

suspicious tumor area while collecting biopsy sample. Primary and metastatic solid tumors contain cancer cells along with normal cells like endothelial cells, fibroblasts and immune/inflammatory cells.[6] Low grade cancer and lack of precision in case of percutaneous biopsy can lead to a normal cell enriched sample with too few of cancer cells. Conventional testing procedure for such a sample is highly time consuming, technically challenging and more likely to reach erroneous conclusions by the pathologist. This paper presents a simpler and straightforward scheme that is capable to recognize a very few cancerous cells from thousands of normal healthy cells, does not require an expert/pathologist and provides statistical comparison based on behavior of each single cell present in the biopsied sample.

Mechanical properties like elasticity, size, viscosity, deformability, and stiffness of the cells stem from the cytoskeleton which is an internal polymer network. It defines the shape of a cell, its mechanical strength and important cellular functions.[7, 8] Cell division, locomotion and transport of intracellular signals are also tightly coupled with the cytoskeleton.[9] Tumor cells differ from normal cells in various aspects including morphology, cell growth, cell-to-cell interactions and cytoskeletal organization.[10-13] Changes to cellular functions and morphology of these diseased cells are mirrored in the cytoskeleton.[14] Consequently, the diseased cells exhibit different mechanical behaviors which indicate the physiological status of the cells and can be used as inherent cell markers for the discrimination of cancerous cells.[15]

To date, just a few experimental techniques have been used to study cellular mechanical properties. Micropipette aspiration is one of the prevailing techniques which applies a negative pressure to the cell and records the aspiration distance as a function

of time.[16] Optical deformability, scanning force microscopy, optical tweezers, hydrodynamic stretching, microplate manipulation and acoustic microscopy have also been reported to determine the cell rigidity.[14, 17-21] All these techniques have revealed cancerous cells to be softer and less resistant to flow under applied forces. Bladder cancer cells have been reported to be as much as 32 times softer than the normal cells using scanning force microscopy.[15] Exceedingly different viscoelastic nature of bladder cancer cells makes these a strong candidate for undertaking elasticity as an inherent cell marker to distinguish the tumor cells from the healthy ones. Metastatic cancer cells display even higher flexibility which stems from their need to squeeze through the surrounding tissue matrix for making their way into the circulatory system.[16, 22] These discoveries show the possible use of cellular elasticity as a robust cell marker to diagnose the underlying disease. But all of the present techniques are limited by poor statistical differentiation, low throughput, high cost, need for special preparation, non-physiological handling or cell adhesion due to mechanical contact of the probe.

Solid-state micropores have been used in a variety of sensor applications, e.g. electroporation, patch clamp measurements, measuring stability of lipid bilayers, monitoring bacterial activities, investigating cell deformability, size based discrimination, cell counting and measuring electric properties of a single cell.[23-28] Chemical and thermal robustness, mechanical strength and capability to be integrated in a lab-on-a-chip system enable micropores to be used for such diverse studies. Though micropores have been reported for investigating cell deformability or detecting large circulating tumor cells (CTCs) present in blood but these have never been reported for diagnosing cancerous cells based on merely cell mechanics discrimination between similar sized

cells. Here, we show single solid-state micropore used as biological transducer that translates the cell mechanics to electrical signals. A single micropore on a membrane sandwiched by a dual compartment setup was used to record the electrical signature of the single cell translocated through the micropore. The specific pulse characteristics distinguished the cancerous cells from healthy ones and provided a statistical differentiation of each translocated cell in a high throughput fashion. This is a simple and dependable scheme to diagnose bladder cancer. Our device not only evaluates the mechanical properties of cells for correlated detection of cancer cells but also uses behavior of every single cell in the statistical analysis.

Materials and Methods

Fabrication of Micropore Device

All the chemicals were obtained from Sigma-Aldrich (St Louis, MO, USA) unless mentioned otherwise. The fabrication process started with a double-side polished, (100) orientation silicon wafer. After standard RCA cleaning of the wafer, a 200 nm thick oxide layer was thermally grown on it (Figure 1). Positive photoresist (Shipley S1813) was spin coated at 4000 rpm for 1 min to get uniformly thick layer of photoresist (~1.2 μm). The photoresist was exposed at 20mJ/sec for 7 sec and developed for 40 sec in MF-319 developer to obtain square windows patterned on one side of the wafer. The other side (bottom side) of the wafer was manually coated with photoresist to shield the oxide from getting etched in subsequent exposure to buffered hydrofluoric (BHF) acid. The square window pattern was transferred to the underlying oxide layer with BHF etch and then acetone was used to remove the residual photoresist from both sides of the wafer. The wafer was immersed in diluted (25%) tetramethylammonium hydroxide (TMAH) at

90 ^{o}C for anisotropic wet etching of silicon. The silicon wafer was etched (etch rate: 1 μm/min) through the whole thickness with sidewall angle of 54.7° until oxide layer on the other side was reached to give oxide membranes. These thin oxide membrane had wavy topography which was due to the internal stresses as shown in Figure 2(a). A micropore of 20 μm diameter was drilled in each thin oxide membrane using the focused ion beam (FIB). The size of the drilled micropore depended on the FIB milling current, thickness of the membrane, material of the membrane and the drilling time.[28-30] Higher the exposure time or the milling current, larger was the diameter of the resulting micropore. An optimized FIB dose (30 kV acceleration voltage, 1 nA milling current, and 260 second exposure time) was used to drill 20 μm micropores in 200 nm thick oxide membranes. SEM micrograph of the drilled micropore revealed that the periphery of the micropore was rough which could rupture the cell membrane during translocation. Thermal treatment of micropores at 1050 °C for 5 minutes not only helped to make the inner walls of the micropore smoother and flat but also removed the residual stress of oxide membrane. Figure 2(b) shows the micrograph of a relaxed and smoothed out micropore after annealing.

Flow of Cells through Micropore

The electrophoretic bias alone was not strong enough to make cells translocate through micropores, as is the case in DNA translocation studies with nanopores. Therefore, an optimized fluid pressure was used to push the cells through the micropore. The ionic current flow through the micropore was continuously monitored and physical blockage of the micropore resulted in distinctive pulses in the temporal current traces. Pulse magnitude, width and shape indicated the biomechanical properties of the translocated

cells and provided the quantifiable viscoelastic behavior of each single cell which distinctively correlated to the physiological status of the cell.

Experimental Setup for Electronic Fingerprinting of Cells

Figure 3 shows the experimental setup. Two Teflon blocks were used to sandwich the micropore chip. Each block had a small channel ending in 1 mm opening which aligned when the blocks were assembled together. The micropore chip was held in place between the two blocks using gaskets made of polydimethylsiloxane (PDMS; Dow Corning). These gaskets restricted leaking of NaCl solution (0.85% w/v) which was used to fill the compartments. Ag/AgCl electrode pair was used to measure the ionic current flow across the micropore. Data acquisition cards (National Instruments) connected to these electrodes provided voltage biasing and recorded the ionic current. A tubing adapter appended the inlet compartment of the Teflon block assembly to a syringe pump (Harvard Apparatus). The syringe pump injected the cells suspended in NaCl solution into the inlet compartment at an optimal flow rate while the outlet compartment was filled with NaCl solution only. Polypropylene cell strainer (BD Falcon) with a nylon mesh (100 μm size) was used to obtain a more uniform single cell suspension and to eliminate any chunks or cell clumps. This was the only pre-processing done to cell samples. When a cell translocated through the micropore, physical blockage of the micropore offered more resistance to the flow of ionic current. Resistance to the flow of current is given by $R = \rho L/A$ where ρ is the resistivity of NaCl (0.85% w/v) solution, L represents the thickness of oxide membrane (length of the micropore) and A stands for the effective area of the micropore. Therefore, any variation

to the effective area of the micropore due to physical blockage by translocating cells was mirrored in its resistance.

PDMS Microchannels to Study Cell Migration

PDMS microchannel devices were fabricated using soft lithography.[31] Each device had 150 μm deep inlet and outlet reservoirs which were connected through an array of 300 tapered micro-channels (from 20 × 5 μm^2 to 5 × 5 μm^2). Initially, photolithography was done to define patterns on master mold which was then used to transfer patterns into PDMS. After punching the fluidic ports, the PDMS device was sterilized, treated with UV ozone plasma for 5 minutes and bonded to sterilized glass coverslip. Equal numbers of cells (50,000 per device) were seeded in the inlet reservoir and were kept inside the incubator in controlled environment (37 ^oC, 5% CO_2 and 95% air) to keep the cells viable. The media was changed periodically, generally within 48 hours. This ensured there was no build up of nutrient gradient across the channels and amongst the cell types. The cells were allowed to migrate through the microchannels without any chemical gradient or external stimuli. Optical micrographs of migrating cells were captured at regular intervals up to 4 days (Figure 4(a)). The number of cells that migrated through the tapered micro-channels and transited to the outlet reservoir over the same length of time were quantified to compare the viscoelastic nature of bladder cancer cells to normal urothelial cells as shown in Figure 4(b).

Culture of Normal Human Urothelial Cells

Immortalized normal human urothelial cells were cultured with T-medium (Invitrogen) supplemented with 5% fetal bovine serum. Cultured normal human

urothelial cells appeared as an epithelioid cell monolayer and were enzymatically dissociated with trypsin (0.25%)-EDTA (0.03%) solution for the experiments.

Culture of Human Bladder Cancer Cell Line

Human bladder cancer cells (T24) were purchased from American Type Culture Collection (Rockville, MD) and cultured with T-medium supplemented with 5% fetal bovine serum. Once bladder cancer cells were confluent, trypsin (0.25%)-EDTA (0.03%) solution was used to dissociate the cells enzymatically in order to acquire cells for the experiments. Typically, Trypan Blue assay was used to assess the viability of the cultured cells after trypsinization and generally >94% cells were found healthy.

Results and Discussion

All the trypsinized cells assumed spherical shape in suspension and were found healthy after disaggregation. The optical micrographs for both the cell types (shown in Figure 5) demonstrated that bladder cancer cells were nearly equal in size to normal urothelial cells. The average diameter for both the cell types was calculated to be in the range of 20-25 um. It dictated that size-based discrimination should be incapable to distinguish between the two types. Figure 4(a) shows that quite a large number of bladder cancer cells could manage to enter the microchannels. These quickly migrated through the channels and exited to the outlet reservoir over a period of 96 hours. On the other hand, normal human urothelial cells couldn't even enter the same microchannels in the same time span. This might be due to the flexible cytoskeleton of malignant cells stemming from their faster replication and enhanced motility.[14] There was no chemical gradient across the channel, however, cancer cells could create

gradient around themselves (micro-gradient) for several reasons such as fast proliferation and fast consumption of medium as compared to the normal healthy cells. This potential gradient might have initiated the cells' vigorous migration into the tapered microchannels. However, once the cells reached the confined space (e.g., 8-5 μm width microchannel), the cells could not divide anymore, due to limited space. The cells with capability to dramatically deform their shape vigorously migrated out toward the other side whereas rigid cells could not migrate through the confined space. We have observed approximately 18 times more cancerous cells in the outlet reservoir as compared to normal urothelial cells after 96 hours, which revealed a clear disparity in their morphological flexibility and mobility. Thus, cellular rigidity reflected the physiological status of the cells and showed the power of the presented approach in detecting diseased cells.

Dual compartment micropore device was assembled as explained in Materials and Methods section. The membrane thickness, micropore size, flow rate and sampling frequency were tuned and tweaked to confine one cell at a time travelling through the micropore and to record the mechanical behavior of every single cell of the sample. Thin silicon dioxide membrane (200 nm) guaranteed single cell translocation through the micropore at any specific time. Micropores less than 12 μm diameter didn't allow the normal urothelial cells to pass through easily and were prone to blockage. On the other hand, micropores larger than 25 μm missed some translocation events so 20 μm diameter micropore size was selected for its enhanced discrimination without getting blocked. An optimized flow rate of 20 μl per minute was selected to achieve maximum throughput without losing any cell translocation events. Similarly, electrical signal

sampling frequency was optimized. High sampling frequency induced a lot of inherent noise which could suppress some current blockage signals during translocation. Lower frequency provided a more stable baseline with less noise but events with translocation times less than the sampling interval could be missed. The optimum ionic current sampling frequency was chosen to be 0.2 MHz which means that electrical signal collection occurred after every 5 µsec. A 5 volt bias was applied across micropore resulting in a 25 MV m^{-1} transmembrane field across the 200 nm long channel. The field would be present only in the locality of the membrane and would not build any gradient in the bulk solution.[32] The cell's microenvironment was not affected by this electric field because fast translocation events were too quick to cause any in-situ damage to the cells. The cells were examined after translocation through the device and were seen to retain their structural properties and looked similar to unprocessed ones.

Phosphate buffered saline (PBS) and 0.85 percent NaCl are commonly used physiological solutions for cell suspension.[28, 33, 34] We suspended the cells in NaCl (0.85% w/v) solution because Ag/AgCl electrodes started losing their AgCl coating in PBS, which was obvious by the whitish end of electrodes dipped in PBS. The gradual loss of AgCl coating caused an unstable baseline but NaCl solution resolved this issue by providing enough Cl^- ions for Ag to retain the AgCl coating on it. The thickness of the oxide membrane defined the area of contact of the cell membrane with the inner walls of the micropore. Micropores of same size but different membrane thickness (200, 330 and 450 nm) were used to study its impact on the translocation behavior of cells. The translocation profile was not much affected by varying the thickness of the membrane but thicker membranes were found to be more prone to blockage/clogging of the

micropore (data not shown). Longer channels provided more area for physical contact between tranlocating cell and the hydrophilic micropore walls. This increased the probability of the hydrophilic phosphate heads of lipid bilayers on cell walls to adhere to the micropore walls. This caused plugging of the micropore. Thus thinner oxide membrane (200 nm) not only ensured single cell measurement but also removed the possibility of micropore clogging while providing enough mechanical strength to be used for multiple runs of the experiment.

Different concentrations of bladder cancer cells were used to record the electronic fingerprints of each single cell in the sample. Figure 6(a) represents the electrical signal trace for a high concentration (20000 cells per ml) and a very low concentration of cells (100 cells per ml). The frequency of translocation events reflects the cell concentration and can be used for cell counting. The frequency of pulses increases linearly with an increase in the cell concentration regardless of the cell type.[28] The translocation profile was found to be steady throughout the measurements regardless of the cell suspension concentration. Figure 6(b) shows the electrical signal profile at different time points (1, 10 and 30 minutes) of the recorded data. This showed that the micropore stayed open and viable for the measurements.

To distinctively identify and quantify the cells from ionic current fluctuations, the cell suspensions were “processed” through the micropore. Equal concentrations (20,000 per ml) of bladder cancer cells and normal urothelial cells were suspended in separate solutions which were processed for 30 minutes in separate runs. The experiments were repeated at least three times and similar results were seen. The data showed characteristically different translocation profiles for the two types of cell suspensions as

shown in Figure 7(a). The cells gave distinctive current blockage pulses (Figures 7(b), 7(c)). Although cell strainer was used earlier (the only pre-processing step on trypsinized cells) to remove cell clots, but still a few of the cells were seen clumped together which were easily recognized from their current blockage pulse shape as demonstrated in Figure 7(d). These pulses were discarded from data analysis so that translocation profiles for only single cells could be compared. When the cancerous cells passed through the micropore, these squeezed due to their deformable nature and translocated through the 20 μm micropore in much smaller time in contrast to their normal counterparts. Rapid translocation events for some of the quickly passing cancerous cells may not have been recorded at 0.2 MHz sampling frequency and even if these were measured, their pulse height might have been imprecise. Given the average translocation time of ~8 μs and sampling interval of 5 μs, there is possibility that some pulses were below the Nyquist limit and got excluded from the analysis. If we would add those pulses to the analyses, the data of Fig. 7(a) and Fig. 8 would be slightly skewed to the left. In spite of this, more than 90% of bladder cancer cells were distinctively identifiable from normal urothelial cells by their pulse characteristics (width, amplitude, pulse shape). Though both the cell types were not much different in size yet normal urothelial cells showed one order of magnitude increase in translocation time owing to their stiffer nature.

The pulse shape can explicitly describe the orientation of the translocating entity.[28, 35] The ionic current through the micropore corresponded to a cross-sectional circular contour which portrayed the particular physical dimension of the confined cell. The outline of translocated cell predominately defined the pulse shape whereas cell's

biomechanical properties characterized its translocation profile. The pulse statistics (average translocation time and peak amplitude) for the two cell types are shown in Table I. The average values were calculated based on thousands of pulse signals for each particular cell type. The reproducibility of the data was verified by repeating the experiments at least three times by using different micropores of same size and similar results were observed when processed at optimized conditions. Statistical analysis based on translocation time and the peak amplitude was performed using one-way ANOVA for independent samples and it demonstrated that the two types were significantly different from each other (p-value < 0.001).

Again, although statistical analysis showed that the two cell types were significantly different in terms of their transit times as well as peak amplitudes but discrimination of cancerous cells was more related to distinction in translocation time (one order of magnitude difference) than the peak amplitude. Therefore, detection efficiency of the system was not notably affected by the artifacts resulting from peak amplitude recorded for pulses that were below the Nyquist limit, that would slightly skew the data towards lower peak amplitude side. The higher sampling frequency could provide more accurate peak amplitudes for faster events but it would increase the background noise affecting the sensitivity of the device by suppressing the smaller current blockage signals (in the range of 1-2 μsec). So here lies the old question of sensitivity versus selectivity. The sampling frequency of 0.2 MHz was optimized with all other experimental process parameters to have a high sensitivity of about 92% and a detection efficiency of 75%.

The normal human urothelial cells showed a greater spread of data because plugging effect of the stiffer cells gave jolted and fluctuated pulses. The micropore not only discriminated the cancerous cells but also provided adequate information to exactly trail the 3D profile of the translocated cell.

Table 1 Summary of pulse statistics for both cell types through 20 μm micropore

Cell Types □ Measurement (Units) □	Bladder Cancer Cells	Normal Urothelial Cells
Average Translocation Time (μsec)	8.48 ± 3.45	107 ± 89.06
Average Peak Amplitude (μA)	3.11 ± 1.04	5.64 ± 2.15

After defining the pulse characteristics (pulse duration, peak amplitude, pulse shape) for each cell type, the bladder cancer cells were mixed with normal urothelial cells at different concentration ratios (1:1, 1:10, 1:100, 1:1000) to detect the presence of cancerous cells out of the mixture. The data was recorded at optimized flow rate (20 μl min^{-1}) and sampling interval (5 μsec). Density plots were drawn to analyze the data distribution (Figure 8). The dashed oval indicates the region designated to the electrical profiles of cancer cells determined from the pulse distribution shown in Figure 7(a). The data showed that translocation profiles for more than 75% of cancer cells spiked in mixed suspension were found in the defined area. It signified that our device could

identify the cancerous cells with a detection efficiency of ~75%, an important metric needed for biopsy samples. The device is thus capable to sense abnormal cells when these are only hundred cancer cells mixed with thousands of normal cells which might be the possible cell population in a biopsy sample collected by FNA.

Though biopsy samples are very important sources for diagnosing cancer but conventional pathology faces high probability for false results and lack of statistical confidence. The presented approach has the potential to overcome many shortcomings by detecting cancer cells without relying on biomarkers, cell staining or experience. Moreover, the device is also capable to diagnose cancer at earlier stage by screening each individual cell of biopsied sample which is almost impossible in standard pathological testing. The recording of cell translocation pulses provides information about cell properties and the analysis gives an affirmative determination of cancer cells. One order of magnitude difference in translocation time dictates the device capability to undertake the highly intrinsic biomechanical properties of a cell as a robust discriminating factor for early detection of cancer. The device can also be used for cell enumeration and phenotype characterization of investigated cells.

Conclusions

A novel approach to identify bladder cancer cells using solid-state micropores as the biological transducer is reported. Biophysical properties (cellular functions, physical dimensions, rigidity, growth rate, cytoskeleton) of cancer cells significantly varied from normal cells. PDMS microchannels also attested significant difference in viscoelastic nature of bladder cancer cells and normal urothelial cells. The micropore device recorded the current blockage pulse for the translocated cell. The data discriminated the

cancer cells from the statistical analysis based on the behavior of every cell in the investigated sample. High throughput, rapid detection, low cost, statistical validity, reliability, no need for cell staining and utility of an inherent cell marker made this device a better alternative for early cancer diagnosis, while also offering a new window into other cellular processes that involve the mechanical properties of cytoskeleton.

Acknowledgments

We would like to thank M. R. Hasan for assistance with graphics and M. A. I. Mahmood for helpful remarks and discussions. The work was supported by grant from the National Science Foundation (ECCS-1201878) to S. M. Iqbal. Azhar Ilyas acknowledges fellowship support from the Cancer Research Foundation of Noth Texas, Arlington, Texas, USA.

References

1. R. G. Sheiman, C. Fey, M. McNicholas and V. Raptopoulos, *AJR. American Journal of Roentgenology*, 1998, **170**, 1603-1607.
2. V. Jeevanandam, M. R. Treat and K. A. Forde, *Gastrointestinal endoscopy*, 1987, **33**, 370-371.
3. J. Melrose, S. Smith and P. Ghosh, in *Cartilage and Osteoarthritis*, Springer, 2004, pp. 39-63.
4. W. Bruening, J. Fontanarosa, K. Tipton, J. R. Treadwell, J. Launders and K. Schoelles, *Annals of Internal Medicine*, 2010, **152**, 238-246.
5. J. B. Haun, C. M. Castro, R. Wang, V. M. Peterson, B. S. Marinelli, H. Lee and R. Weissleder, *Science Translational Medicine*, 2011, **3**, 71ra16.
6. L. Y. Joanne and J. W. Rak, *Breast Cancer Res*, 2003, **5**, 83-88.
7. E. L. Elson, *Annual Review of Biophysics and Biophysical Chemistry*, 1988, **17**, 397-430.
8. H. Lodish, A. Berk, S. L. Zipursky, P. Matsudaira, D. Baltimore and J. Darnell, *Molecular Cell Biology*, W. H. Freeman, New York, 1999.
9. P. Janmey, *Handbook of Biological Physics*, 1995, **1**, 805-849.
10. K. Rao and H. J. Cohen, *Mutation Research/DNAging*, 1991, **256**, 139-148.
11. A. Ben-Ze'ev, *Biochimica et Biophysica Acta (BBA)-Reviews on Cancer*, 1985, **780**, 197-212.
12. H. Yamaguchi and J. Condeelis, *Biochimica et Biophysica Acta (BBA)-Molecular Cell Research*, 2007, **1773**, 642-652.
13. M. Yilmaz and G. Christofori, *Cancer and Metastasis Reviews*, 2009, **28**, 15-33.

14. J. Guck, S. Schinkinger, B. Lincoln, F. Wottawah, S. Ebert, M. Romeyke, D. Lenz, H. M. Erickson, R. Ananthakrishnan and D. Mitchell, *Biophysical Journal*, 2005, **88**, 3689-3698.

15. M. Lekka, P. Laidler, D. Gil, J. Lekki, Z. Stachura and A. Z. Hrynkiewicz, *European Biophysics Journal*, 1999, **28**, 312-316.

16. K. A. Ward, W. I. Li, S. Zimmer and T. Davis, *Biorheology*, 1991, **28**, 301.

17. M. Radmacher, *Methods in Cell Biology*, 2002, **68**, 67-90.

18. J. Sleep, D. Wilson, R. Simmons and W. Gratzer, *Biophysical Journal*, 1999, **77**, 3085-3095.

19. O. Thoumine and A. Ott, *Biorheology*, 1997, **34**, 309-326.

20. T. Kundu, J. Bereiter-Hahn and I. Karl, *Biophysical Journal*, 2000, **78**, 2270-2279.

21. D. R. Gossett, T. K. Henry, S. A. Lee, Y. Ying, A. G. Lindgren, O. O. Yang, J. Rao, A. T. Clark and D. Di Carlo, *Proceedings of the National Academy of Sciences*, 2012, **109**, 7630-7635.

22. J. B. Wyckoff, J. G. Jones, J. S. Condeelis and J. E. Segall, *Cancer Research*, 2000, **60**, 2504-2511.

23. A. ul Haque, M. Zuberi, R. E. Diaz-Rivera and D. Marshall Porterfield, *Biomedical Microdevices*, 2009, **11**, 1239-1250.

24. B. Matthews and J. W. Judy, *Journal of Microelectromechanical Systems*, 2006, **15**, 214-222.

25. M. Kitta, H. Tanaka and T. Kawai, *Biosensors and Bioelectronics*, 2009, **25**, 931-934.

26. X. Niu and Z. Yan, *Journal of Biomedical Engineering*, 2001, **18**, 615.

27. H. Chang, A. Ikram, F. Kosari, G. Vasmatzis, A. Bhunia and R. Bashir, *Journal of Vacuum Science & Technology B: Microelectronics and Nanometer Structures*, 2002, **20**, 2058-2064.

28. W. Asghar, Y. Wan, A. Ilyas, R. Bachoo, Y. Kim and S. M. Iqbal, *Lab on a Chip*, 2012, **12**, 2345-2352.

29. W. Asghar, A. Ilyas, J. A. Billo and S. M. Iqbal, *Nanoscale Research Letters*, 2011, **6**, 1-6.

30. W. Asghar, A. Ilyas, R. R. Deshmukh, S. Sumitsawan, R. B. Timmons and S. M. Iqbal, *Nanotechnology*, 2011, **22**, 285304.

31. Y. Wan, D. Tamuly, P. B. Allen, Y.-t. Kim, R. Bachoo, A. D. Ellington and S. M. Iqbal, *Biomedical Microdevices*, 2012, 1-9.

32. J. B. Heng, A. Aksimentiev, C. Ho, P. Marks, Y. V. Grinkova, S. Sligar, K. Schulten and G. Timp, *Nano Letters*, 2005, **5**, 1883-1888.

33. L. G. Collste, M. Devonec, Z. Darzynkiewicz, F. Traganos, T. K. Sharpless, W. F. Whitmore and M. R. Melamed, *Cancer*, 1980, **45**, 2389-2394.

34. T. Tansatit, S. Sahaphong, S. Riengrojpitak, V. Viyanant and P. Sobhon, *Veterinary Parasitology*, 2006, **135**, 269-278.

35. P. Chen, J. Gu, E. Brandin, Y. R. Kim, Q. Wang and D. Branton, *Nano Letters*, 2004, **4**, 2293-2298.

List of Figure Captions:

Figure 1. **The process flow for fabrication of solid-state micropores (a)** Thermal oxidation of double-side polished silicon wafer **(b)** Spin-on photoresist followed by conventional photolithography to open square windows in resist layer **(c)** BHF etch to transfer the square window pattern to the underlying oxide layer **(d)** TMAH anisotropic etch of silicon using oxide layer on the other side of the wafer (bottom side) as the etch stop to obtain oxide membrane diaphragms **(e)** Drilling of micropore in the oxide membrane using focused ion beam.

Figure 2. SEM micrographs of (a) Oxide membrane shows wavy surface which is due to the internal stress of the thin film, and (b) A 20 μm micropore after thermal annealing. The membrane is relaxed.

Figure 3. **Experimental setup (a)** Syringe pump pushes the cells to the inlet chamber of Teflon block assembly. The chip with single micropore is sandwiched between the Teflon blocks. PDMS gaskets are used to avoid leakage and Ag/AgCl electrodes are inserted in the tubing appended at the inlet and outlet chambers **(b)** The inner view of Teflon blocks shows PDMS gaskets sealing the micropore chip.

Figure 4. Comparative study of cell migration through the microchannels **(a)** Optical micrographs show that bladder cancer cells are more viscoelastic as compared to normal urothelial cells. Softer nature of bladder cancer cells allow a large number of cells to squeeze and enter the tapered microchannels while rigidity of normal urothelial cells restrain them from entering into same sized microchannels over same length of

time (96 hours) **(b)** Plot demonstrates the quantitative analysis for both types of cells that were able to migrate to outlet reservoir after 96 hours.

Figure 5. Optical micrographs showing bladder cancer cells and normal urothelial cells. The cells are spherical in suspension and are seen to be healthy. These also demonstrate that both types of cells are nearly equal in size (20-25 μm).

Figure 6. Cell concentration and reliability (a) Comparison of the electrical signal for high concentration and low concentration of cell suspension demonstrates that the frequency of pulses reflects the concentration and can be used for cell enumeration **(b)** The translocation profile for both cell types remained stable throughout the experiments. The device shows similar current signals at 1, 10 and 30 minutes after initial cell detection for each cell type which indicates the reliability of the device.

Figure 7. Scatter plot and translocation profile of the cells passing through the micropore (a) The distribution of pulses for both types of cells processed separately through the micropore device is shown on a single plot for comparison. The plot indicates that cancer cells show distinctively different electrical profile when compared to their normal counterpart. **(b)** and **(c)** demonstrate characteristic translocation current trace (translocation time, current peak amplitude) for bladder cancer cells and normal urothelial cells respectively. **(d)** The pulse shape clearly shows that the signal is from the cells clumped together. This information is used to eliminate these data points from analysis.

Figure 8. Data density plots for cell suspensions mixed in different ratios. **(a – d)** show data density plots for cell suspension with decreasing relative concentration of

cancer cells **(a)** 1:1 **(b)** 1:10 **(c)** 1:100 **(d)** 1:1000. The cancer cells show distinctive current signal and can be efficiently identified out of a mixed cell suspension as pointed out by the dashed ovals. The color map designates the relative data density distribution of cells.

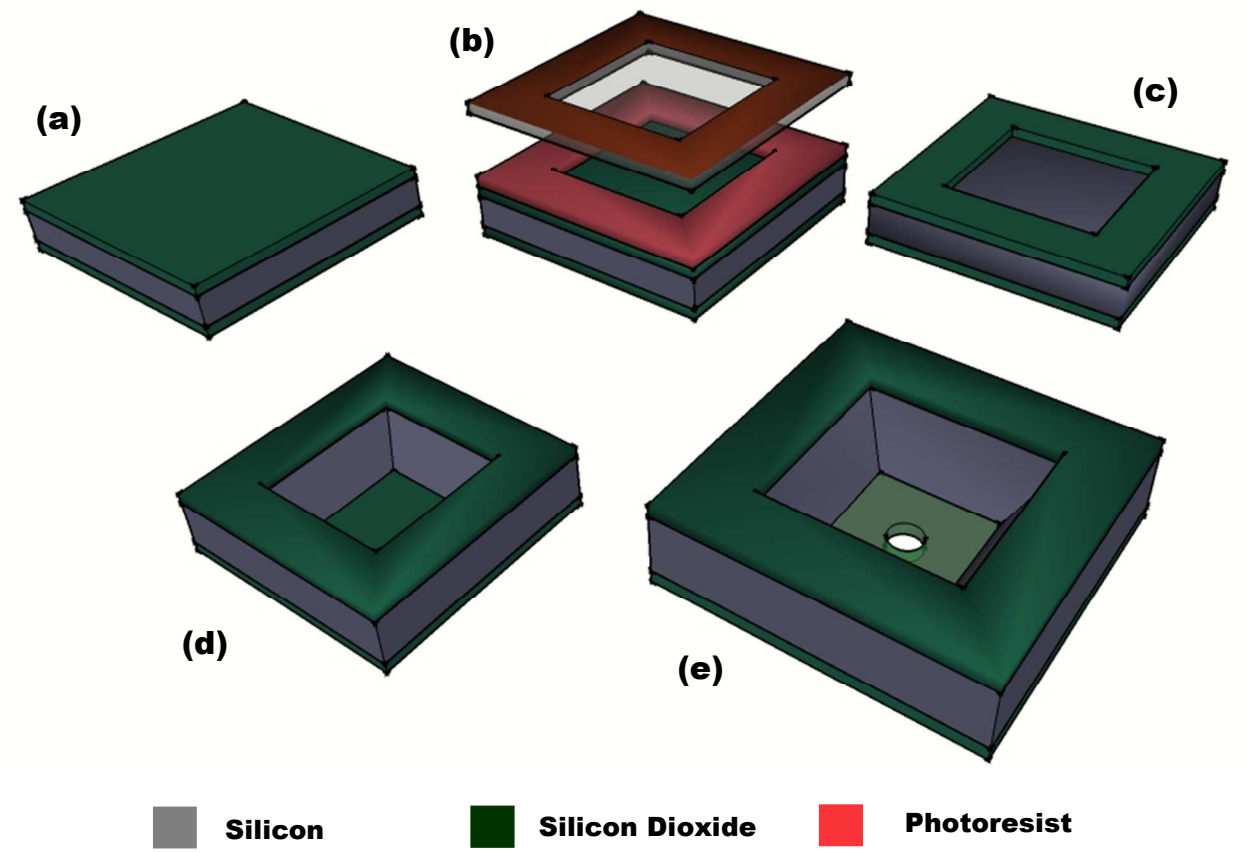

Figure 1

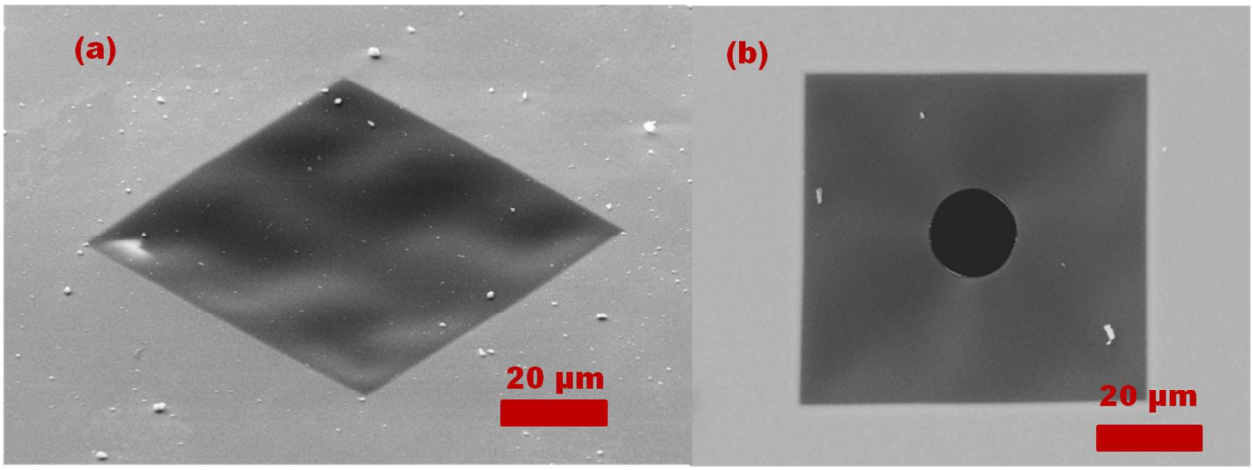

Figure 2

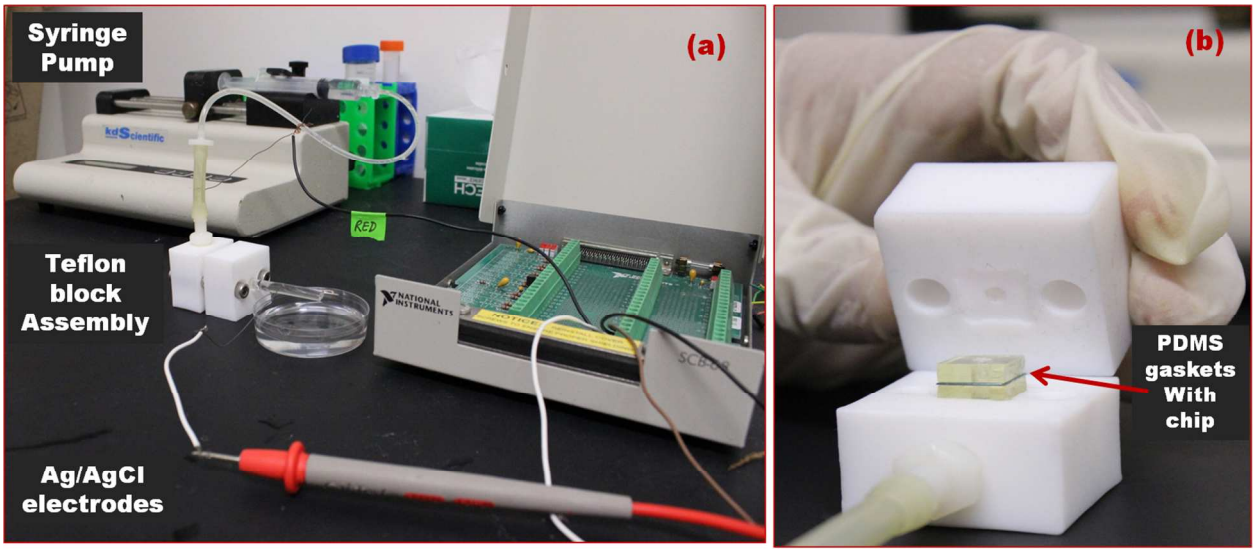

Figure 3

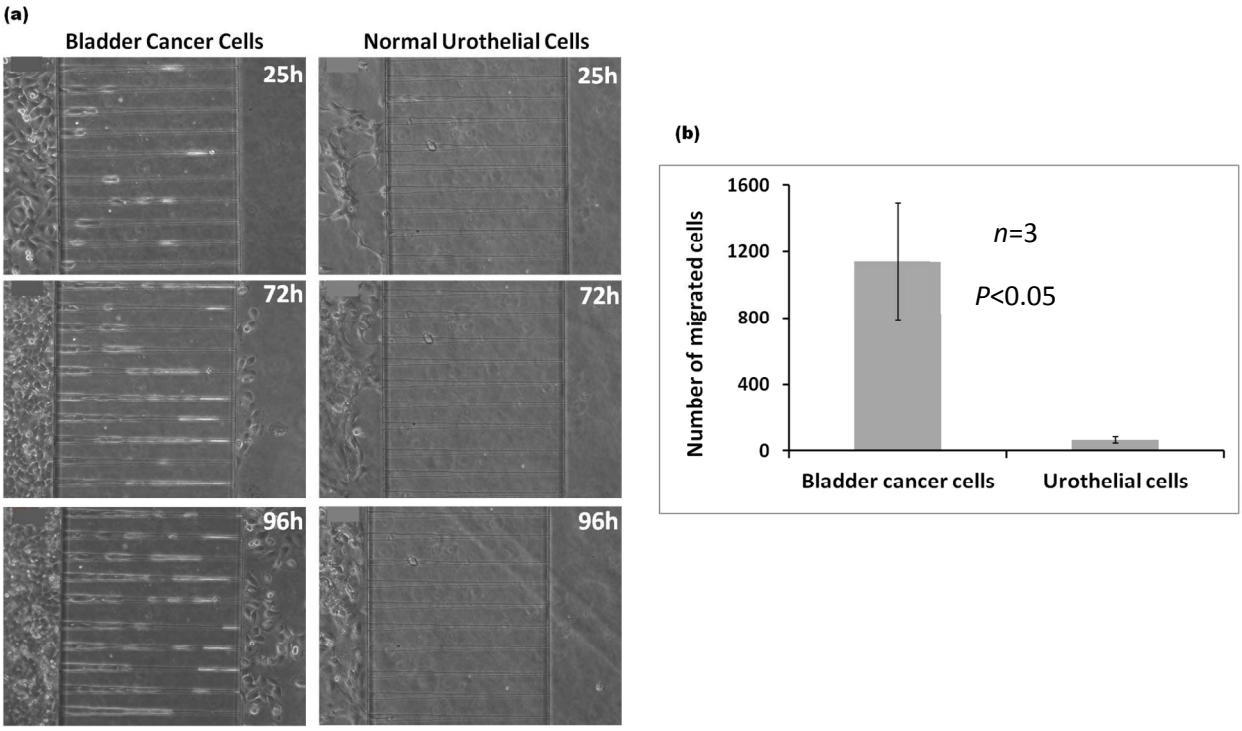

Figure 4

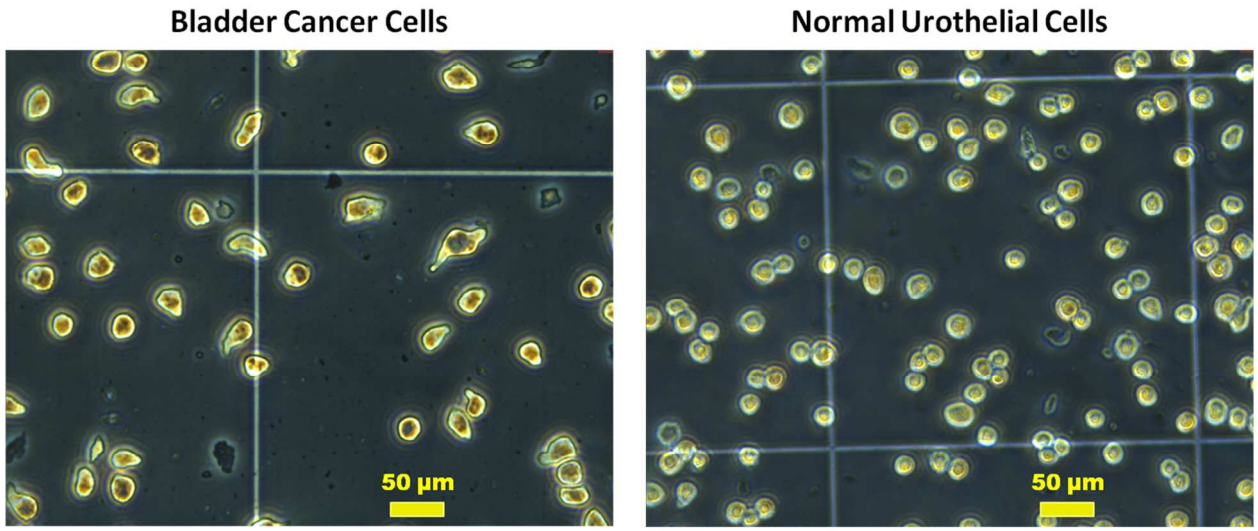

Figure 5

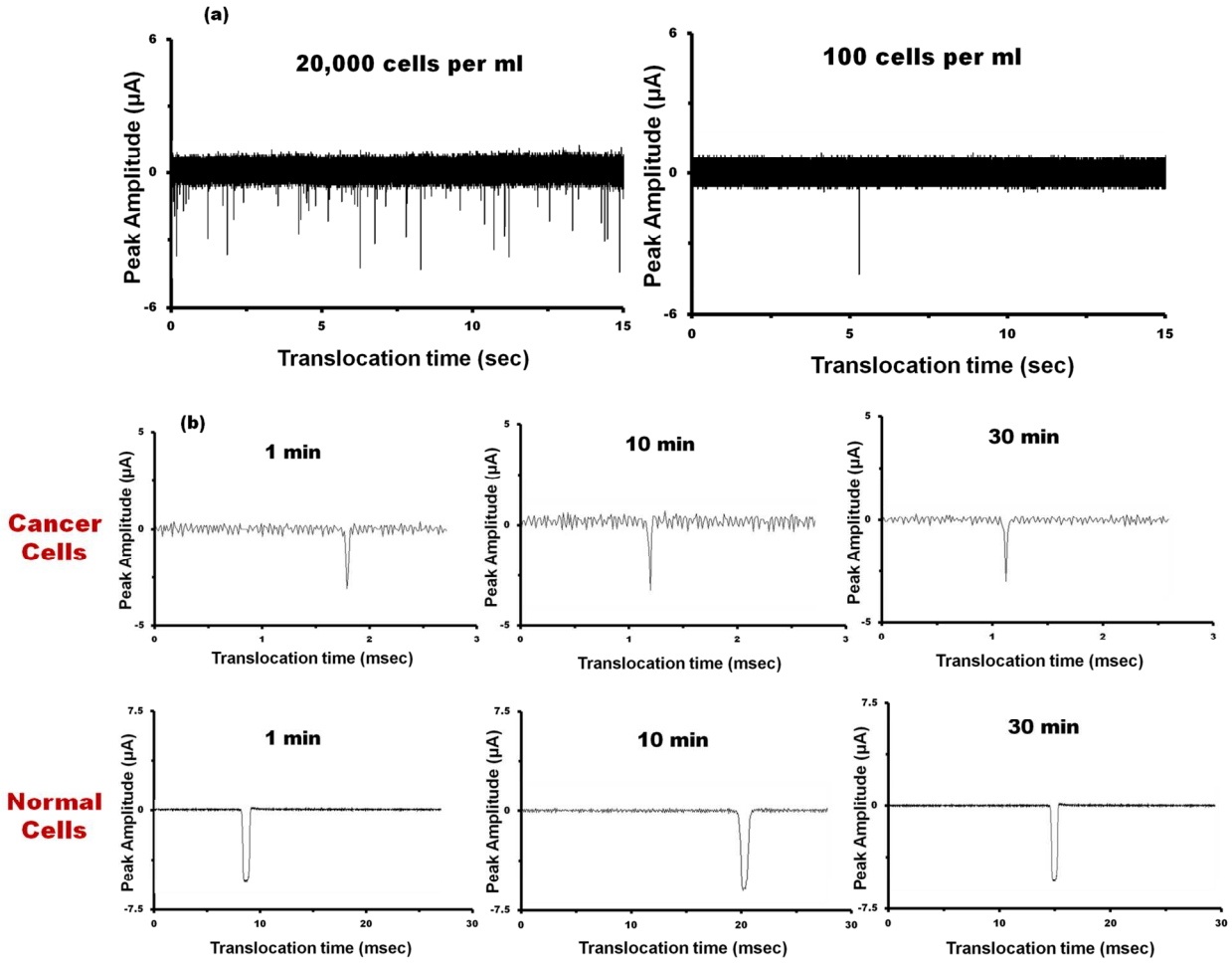

Figure 6

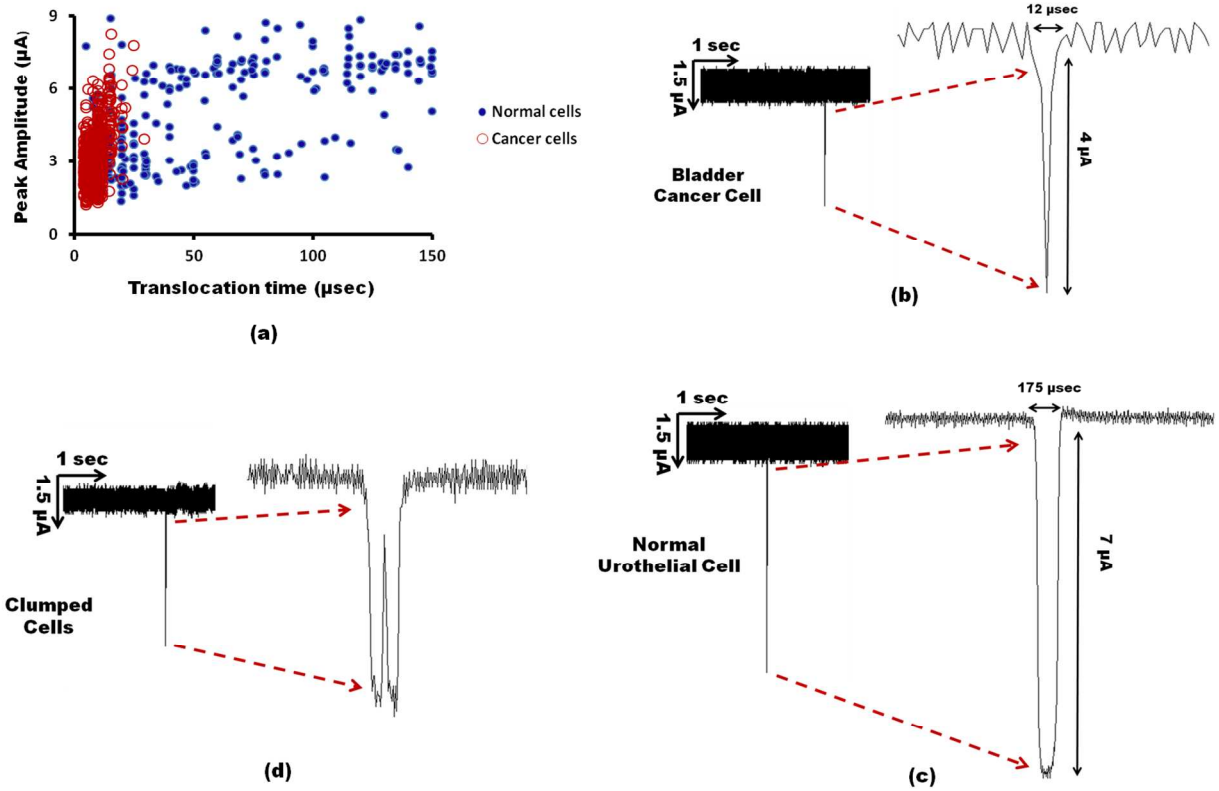

Figure 7

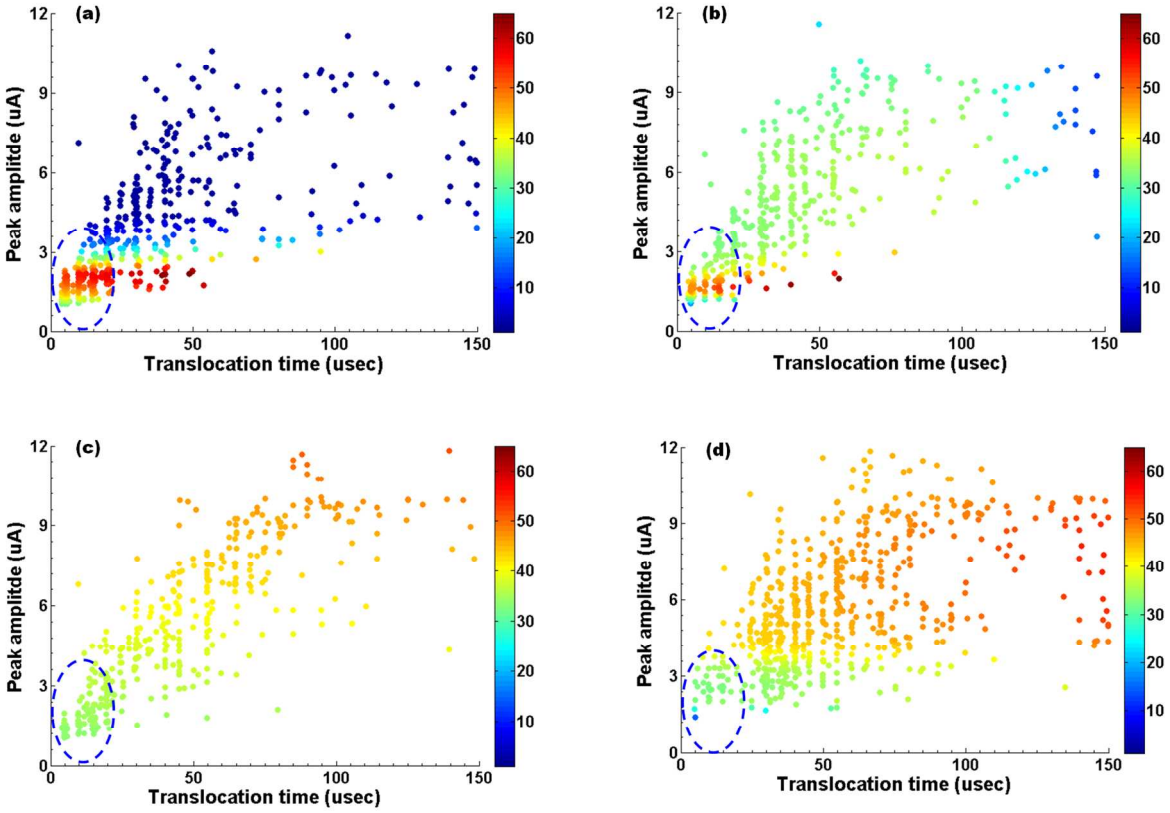

Figure 8